1-1-2016

Experimental Strain Measurement In Ultrasonic Welding Of Battery Tabs

Chen Chen
Wayne State University,

EXPERIMENTAL STRAIN MEASUREMENT IN ULTRASONIC WELDING OF BATTERY TABS

by

CHEN CHEN

Submitted to the Graduate School

of Wayne State University,

Detroit, Michigan

in partial fulfillment of the requirements

for the degree of

MASTER OF SCIENCE

2016

MAJOR: MECHANICAL ENGINEERING

Approved By:

_____

Advisor Date

ACKNOWLEDGEMENTS

I would like to thank my advisor Prof. Chin-An Tan for his guidance, patience, and encouragement during the research work.

I would also like to thank Dr. Bongsu Kang for his help and supports for theoretic vibration study and modeling.

Also thanks to Mr. Ao Yu, for helping me prepared the presentation and given me good advice about data processing. Mr. Harry He, give me encouragement to insist my work during hard times.

Table of Contents

LIST OF TABLES

LIST OF FIGURES

Chapter 1: Introduction

1.1 Lithium Ion Battery Pack Assembly Technology Overview

Electrical drive vehicle becomes more and more popular these years. Battery technology is very important for electrical drive vehicle. Currently, the Lithium ion battery is most popular battery type in many kinds of battery types include Lead-acid battery, Nickel metal hydride battery, and Zebra battery. Typically the battery pack of the electrical drive vehicle composited by hundreds of battery cells connected together to provide enough power for the vehicle. These joints must be robust both in mechanical aspect and electrical aspect. The failure of one joint will result in whole battery pack fail due to an open circuit created by the failed joint. There are many kinds of assembling technologies[1] to build connections between battery cells include laser welding, ultrasonic welding, resistance welding, mechanical joint etc. Among these connection technologies, ultrasonic welding is very popular due to its low cost and ability to connect dissimilar, high conductive metal sheet[2]. For example, the resistance welding cannot work effectively with conductive metals like copper and aluminum. Because of the anodizing and coating on the surface, anodized aluminum battery tab and nickel-coated copper battery tab cannot be welded by laser[3]. Ultrasonic welding is a solid-state joining process[4, 5] which does not require filler material, thus reduces the cost and waste.

1.2 Ultrasonic Welding for Battery Pack Assembly.

The typical set up of battery cell ultrasonic welding shown in Figure 1[3]. Hundreds of battery cells connected through the interconnect board. Multiple layers of battery tabs clamped with bus-bar under pressure between sonotrode and anvil. The piezo-stacks transducer generates ultrasonic oscillation which has the peak vibration amplitude at the sonotrode tip. The amplitude of oscillation typically in the range 5-30 micrometers. The sonotrode tip transfer shear motion between battery tabs, which generates solid bonds between the metal sheets under clamp pressure.

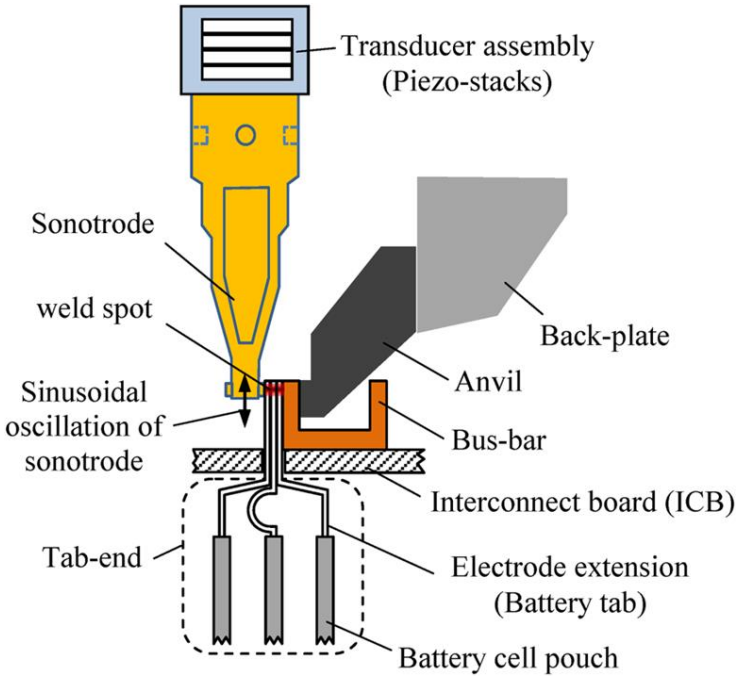

Figure 1 Typical ultrasonic welding set up [3]

The fundamental principle, experimental studies of welding mechanism, and finite element studies for ultrasonic welding are presented by Vries[6],Rozenberg, Mitkevitch[7], Devine[8],Flood[9],Lee[10],Viswanath[11] , Siddiq[12]. The influence of ultrasonic wavelength studied by Lee[13]. And reference [14]shows that the bonding strength of ultrasonic welding

joint is strongly influenced by the vibration of the weld parts. The dynamic and vibration of battery tabs during ultrasonic welding were studied by Kang [3, 15, 16] analytically. Currently, the experimental studies of battery tab dynamic were limited. Hence in this thesis project, experimental measurements of battery tabs dynamic during ultrasonic welding were conducted.

1.3 Damage of Battery during Ultrasonic Welding

The battery tab in a battery cell is a metal sheet which connects components inside of the battery cell to outside battery components such as bus bar. As shown in figure 2. During the ultrasonic welding process to connect the battery tab to bus bar, a critical position in the battery cell sometimes broken. This may cause by the high frequency vibration induced from the ultrasonic welding process. In this study, the mechanism of battery broken during ultrasonic welding was explored.

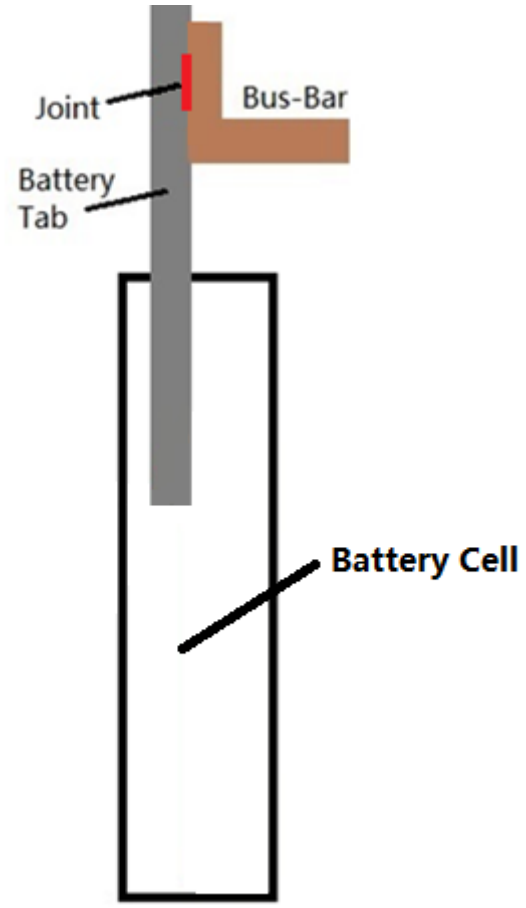

Figure 2 Battery tab connection schematic

1.4 Experimental Measurement System and Objective

To measure the dynamic and vibration of battery tab, several kinds of sensors may be adopted, includes laser vibrometer[17], high speed camera[18], accelerometer[19, 20] etc.. The laser vibrometer can only measure one point flexural vibration of battery tab, high speed camera can only measure the lateral vibration of the battery tab, the accelerometer need to be attached to the battery, and it is too heavy, probably changes the battery tab vibration property. Among those sensors, strain gauge [21-24] as a sensor mounted on metal surface, has the advantage of cheap, and given the accurate result. In this studies, an instrumentation system includes strain gauge sensor, Wheatstone bridge, amplifier and data acquisition equipment has been built for the dynamic measurement purpose.

The objective of this study is testing the analytical model of battery tabs vibration during ultrasonic welding, explore the mechanism of inside battery joint damage during ultrasonic welding.

Chapter 2: Theoretic Analysis of Battery Tab Vibration

2.1 Modeling of Battery Tab Overview:

Due to the shape of the battery, it always needs to bend the battery tab to ‘S’ shape for manufacture assembly purpose. The sonotrode transfer longitudinal vibration to the battery tab, through the ‘S’ bend, part of the longitudinal vibration becomes flexural vibration. In this study, both longitudinal vibration model and flexural vibration model were built to describe the dynamic of the tab. In reference[25] The theory of power ultrasonic was introduced.

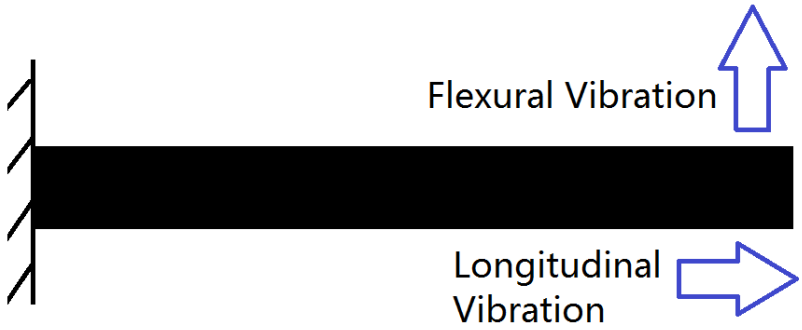

Figure 3 Modeling of battery tab vibration

2.2 Longitudinal Vibration Induced Stress Analysis on Battery Tab:

Model the battery tab as a thin bar. Assume at the welding area, the battery tab has the same displacement as the sonotrode. And at the other end of the battery tab, it was fixed inside the battery. As shown in the picture. At the left hand side where x=0, a harmonic displacement as input to the system. On the right hand side where x=L, the battery has fixed boundary condition.

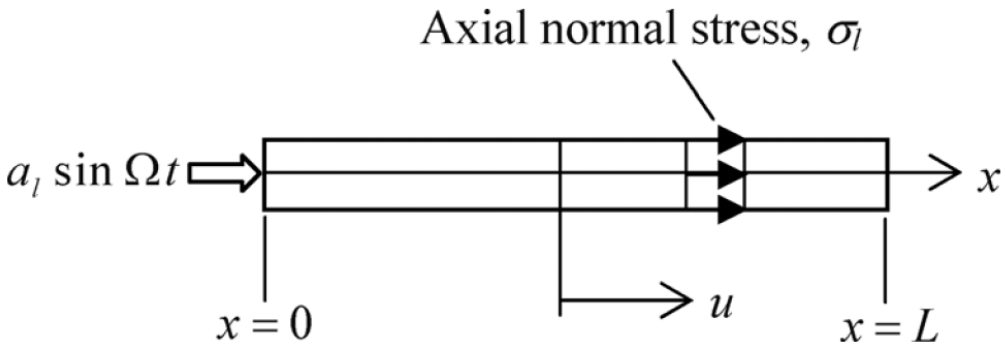

Figure 4 Modeling of battery tab longitudinal vibration[3]

The steady state longitudinal displacement of beam vibration can be expressed as

$$u = (c_1 \cos(\lambda x) + c_2 \sin(\lambda x))(c_3 \cos(\Omega t) + c_4 \sin(\Omega t)) \quad (1)$$

Where λ is the longitudinal wavenumber defined by:

$$\lambda = \Omega / c_0 \qquad c_0 = \sqrt{E/\rho} \quad (2)$$

Apply boundary condition:

$$\text{At x=0, } u = a_l sin\Omega t \qquad \text{at x=L, } u = 0 \quad (3)$$

Then $$u = a_l(\cos(\lambda x) - \cot(\lambda L)\sin(\lambda x))sin\Omega t \quad (4)$$

The axle normal stress distribution along the battery tab will be

$$\sigma_l(x,t) = E\frac{\partial u(x,t)}{\partial x} = -Ea_l\lambda(\sin(\lambda x) + \cot(\lambda L)\cos(\lambda x))\sin(\Omega t) \quad (5)$$

In a similar way, if we assume the tab has free boundary condition on the right hand side, the normal stress can be expressed as

$$\sigma_l(x,t) = E\frac{\partial u(x,t)}{\partial x} = Ea_l\lambda(\tan(\lambda L)\cos(\lambda x) - \sin(\lambda x))\sin(\Omega t) \qquad (6)$$

Define the total length of the battery tab as 1, the length of span 1 as ¼ of the total length. The longitudinal vibration mode shape shows in Figure 5.

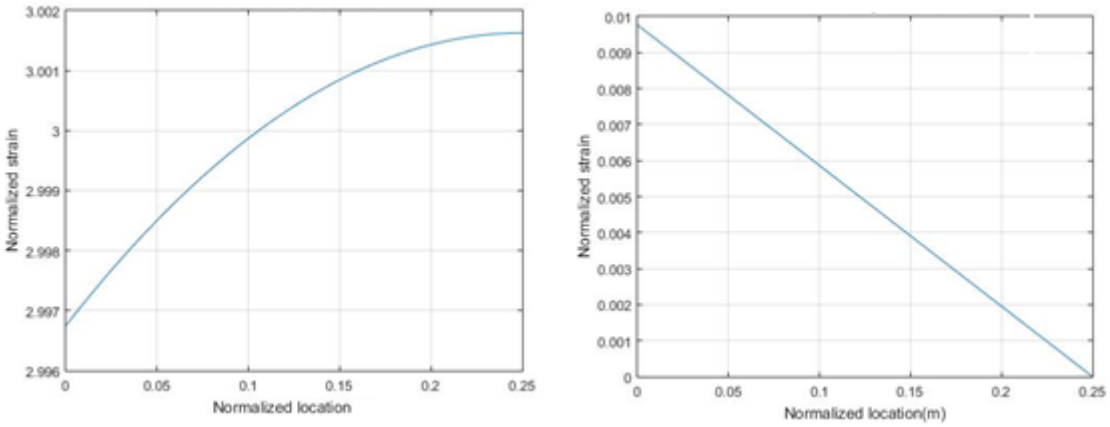

(a) Fixed boundary condition (b) Free boundary condition

Figure 5 Mode shape of battery tab longitudinal vibration

Figure 5 shows that with the same excitation, under the fixed boundary condition the longitudinal vibration induced much more strain than the free boundary condition on the battery tab.

2.3 Flexural Vibration Induced Stress Analysis:

To analysis flexural vibration of battery tab, Consider the battery tab as a thin beam. Subjected to harmonic displacement excitation $a_f \sin(\Omega t)$ at x=0 in the direction perpendicular to the tab, as shown in Figure 6. The vertical displacement from flexural vibration can be assumed as

$$w(x,t) = (C_1 cos\gamma x + C_2 cosh\gamma x + C_3 sin\gamma x + C_4 sinh\gamma x) sin\Omega t \qquad (7)$$

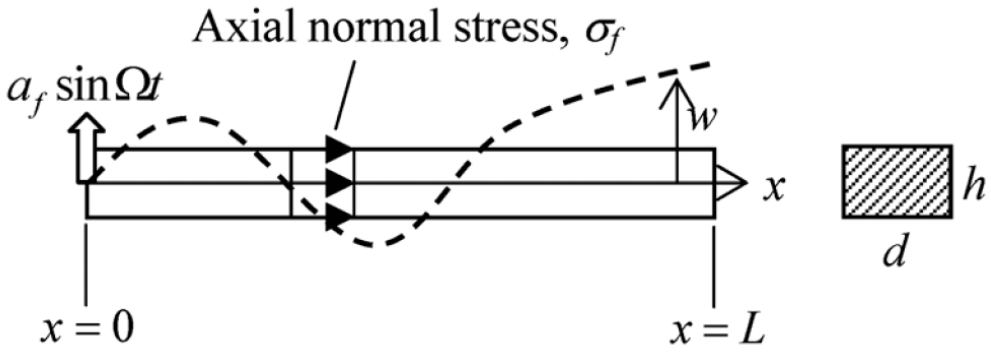

Figure 6 Modeling of battery tab flexural vibration [3]

Where γ represents the flexural wavenumber which is defined as

$$\gamma^2 = \sqrt{\frac{A}{I}\frac{\Omega}{c_0}} \qquad c_0 = \sqrt{\frac{E}{\rho}} \qquad (8)$$

$$\frac{\partial w(x,t)}{\partial x} = \gamma(-C_1 sin\gamma x + C_2 sinh\gamma x + C_3 cos\gamma x + C_4 cosh\gamma x) sin\Omega t \qquad (9)$$

Where $A = dh$ represent the cross section area, $I = dh^3/12$ is second area of inertia of the beam.

Apply boundary condition:

At x=0, due to the excitation and zero slope,

$$w(0,t) = a_f si\, n(\Omega t) \qquad (10)$$

$$\frac{\partial w(0,t)}{\partial x} = 0 \tag{11}$$

Thus $a_f = C_1 + C_2$ $\qquad\qquad$ $0 = C_3 + C_4$

At x=L, the deflection and the derivative of the deflection function is zero

$$w(L,t) = 0 \tag{12}$$

$$\frac{\partial w(L,t)}{\partial x} = 0 \tag{13}$$

Thus

$$C_1 = \frac{a_f[(sin\gamma L - sinh\gamma L)sinh\gamma L - (cos\gamma L - cosh\gamma L)cosh\gamma L]}{(sin\gamma L - sinh\gamma L)(sin\gamma L + sinh\gamma L) + (cos\gamma L - cosh\gamma L)^2} \tag{14}$$

$$C_2 = \frac{a_f[(sin\gamma L - sinh\gamma L)sin\gamma L + (cos\gamma L - cosh\gamma L)cos\gamma L]}{(sin\gamma L - sinh\gamma L)(sin\gamma L + sinh\gamma L) + (cos\gamma L - cosh\gamma L)^2} \tag{15}$$

$$C_3 = \frac{-a_f[cos\gamma L sinh\gamma L + cosh\gamma L sin\gamma L]}{(sin\gamma L - sinh\gamma L)(sin\gamma L + sinh\gamma L) + (cos\gamma L - cosh\gamma L)^2} \tag{16}$$

$$C_4 = \frac{a_f[cos\gamma L sinh\gamma L + cosh\gamma L sin\gamma L]}{(sin\gamma L - sinh\gamma L)(sin\gamma L + sinh\gamma L) + (cos\gamma L - cosh\gamma L)^2} \tag{17}$$

$$w(x,t) = (C_1 cosCx + C_2 cosh\gamma x + C_3 sin\gamma x + C_4 sinh\gamma x) sin\Omega t \tag{18}$$

$$\sigma_f(x,t) = Ez(\partial^2 w(x,t))/\partial x^2$$

$$= \frac{Eh}{2}\gamma^2(-C_1 cos\gamma x + C_2 cosh\gamma x - C_3 sin\gamma x + C_4 sinh\gamma x) sin\Omega t \quad (19)$$

Where $z = \frac{h}{2}$

Making the denominator of C_1, C_2, C_3, C_4 equal to zero, we will find the γL which make the beam vibration resonant.

$$\gamma L = [4.73, 7.853, 10.996, 14.137, 17.279] \quad (20)$$

The battery tab was divided into 3 Span in the length direction as shown in Figure 7. Span 2 and Span 3 has both longitudinal vibration and flexural vibration

Compare the numerical value of battery tab span 3 length, γL is very close to the resonance tab length shown in equation (20). The modeled Span 3 length is between 57.5%-63.5% of the total battery length. As shown in Figure 3, the intersection between Span 2 and Span 3 is a curve with a radius which cannot be neglected. This is the reason why the tab Span 3 length between 57.5%-63.5%. The mode shape with tab length around the real length of span 3 shown in Figure 8.

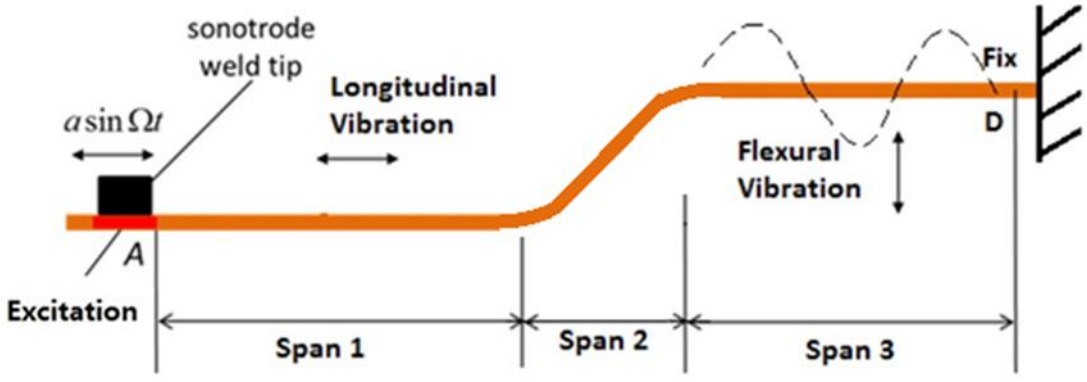

Figure 7 Span schematic of battery tab

The flexural vibration mode shape shown in Figure 8.

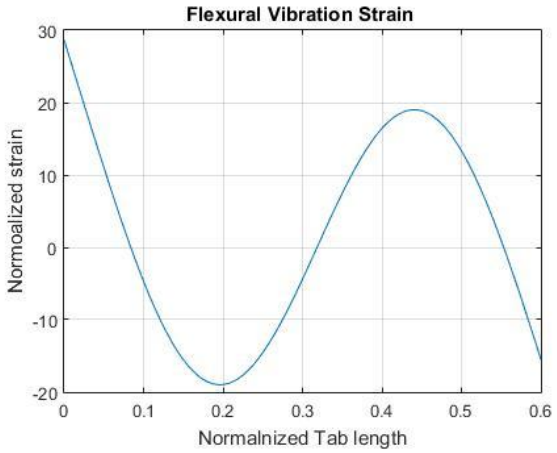

(a) Span 3= 63.5% whole tab length

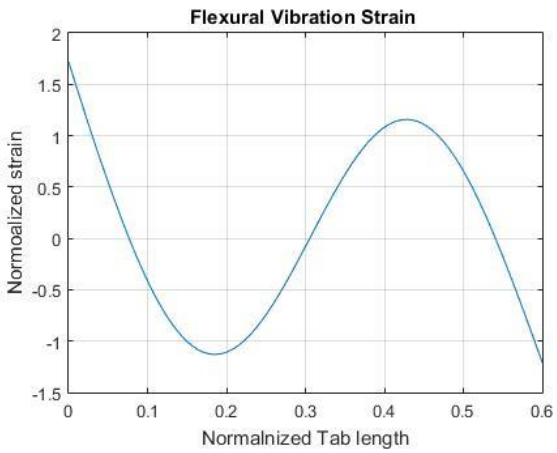

(b) Span 3=62.5% of whole tab length

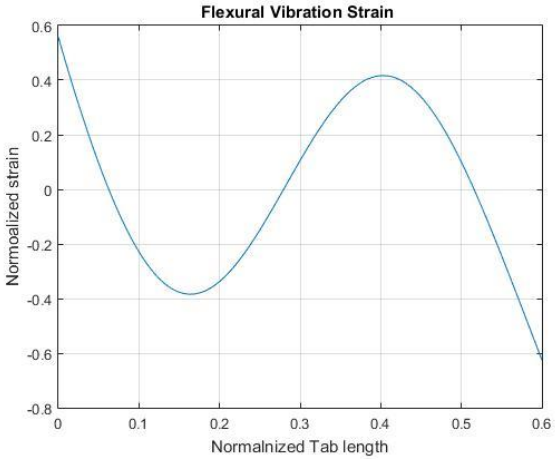

(c) Span 3=60% of whole tab length

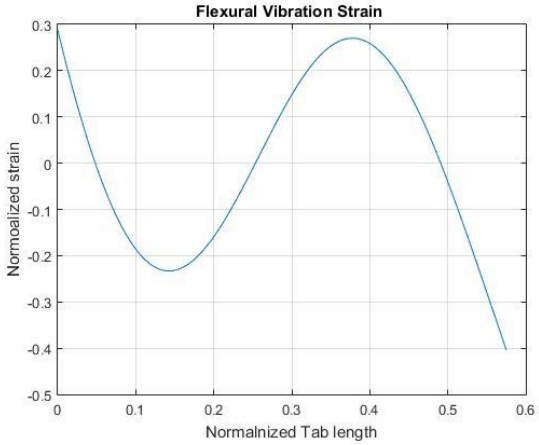

(d) Span 3=57.5% of whole tab length

Figure 8 Mode shape of span 3 flexural vibration

Figure 8 shows that the strain/stress value at Span 3 is sensitive to the Span 3 length. Adjust the length of tab 3 may help to reduce the stress value on the battery tab.

Chapter 3 Instrumentation and Benchmark

3.1 Instrumentation Overview:

In this study, strain gauge was selected as the sensor to measure the battery tab vibration induced strain/stress. Typically, strain gauge was used to measure static strain. However, K. Ueda and A. Umeda's study [26] shows that some kinds of strain gauge can work in dynamic measurements up to 300kHz. In this study, the strain gauge provides by Kyowa Company did not have any dynamic measurement benchmark before. Hence benchmark experiments were carried out to test the capability of the strain gauge sensor. For the signal conditioning and data acquisition system, the commercial system provides by Kyowa Company has following disadvantages: 1. No digital trigger. 2. High Noise (160 micro-strain). 3. Expensive. Hence a study of instrumentation was conducted and a measurement system include signal conditioning and data acquisition was built. This homemade measurement system has following advantages: 1. Cheap 2. Low noise (80 micro-strain) compare with a commercial system from Kyowa Company (200 micro-strain).

The measurement system composed by strain gauge sensor, Wheatstone bridge circuit[27-29], instrumentation amplifier, NI-Precise Power Supply, NI-Data Acquisition modulus. LabVIEW program was built to collect data to Microsoft Excel file. And Matlab software was used to conduct signal processing.

Figure 9 shows the schematic of the measurement system. Strain gauge convert strain signal to resistance, then through Wheatstone bridge convert small resistance signal to voltage output. After amplification the voltage output record by NI data acquisition system.

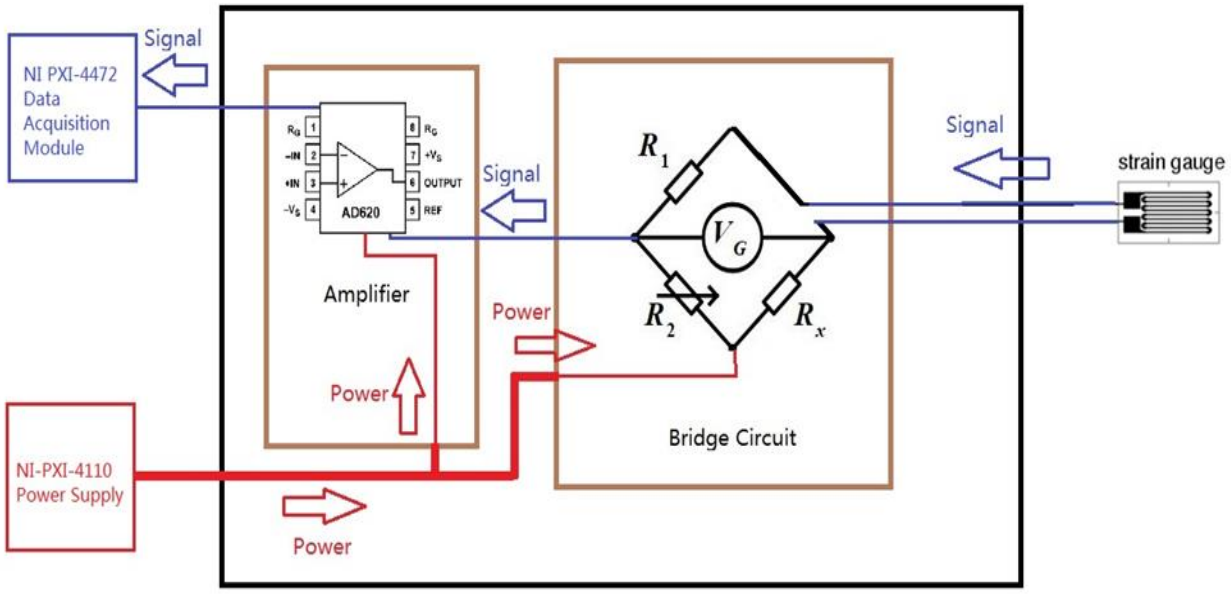

Figure 9 Schematic of measurement instrumentation system

3.2 Study of Strain Gauge Mass Influence to the Battery Tab Dynamic

The battery tab is a thin metal sheet which has small mass which is just several grams. The strain gauge sensor itself is very light, but the cable which connected to the gauge is heavy compared to the battery tab. Hence a study of intermediate mass effect to the battery tab vibration has been conducted.

Longitudinal Vibration of Battery Tab with Lumped Mass:

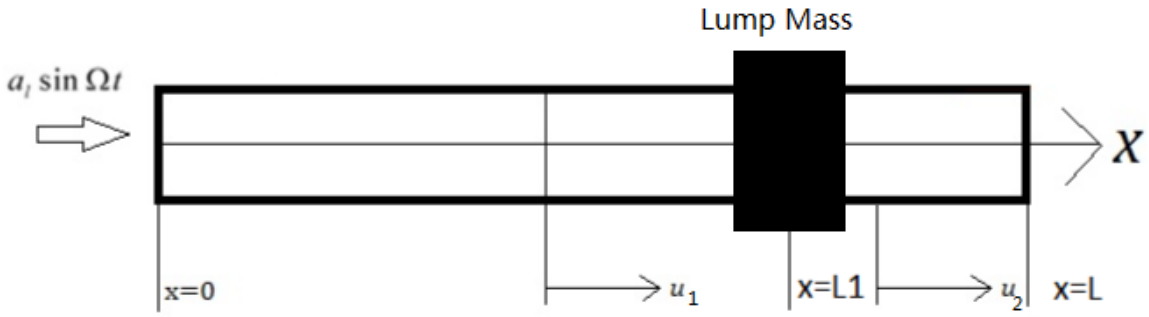

Figure 10 Lumped mass on battery tab

Assume the node displacement

$$u_1 = (c_1 cos\lambda x + c_2 sin\lambda x) \sin \Omega t \qquad (21)$$

$$u_2 = (c_1' cos\lambda x + c_2' sin\lambda x) \sin \Omega t \qquad (22)$$

The boundary condition:

At x=0, $u_1(0,t) = a_l sin\Omega t$ ⇨ $c_1 = a_l$ (23)

At x=L_1,

$$u_1(l_1,t) = u_2(l_1,t) \qquad (24)$$

$$\frac{\partial u_2(l_1,t)}{\partial x}-\frac{\partial u_1(l_1,t)}{\partial x}=\frac{M}{EA}\frac{\partial^2 u(l_1,t)}{\partial t^2} \tag{25}$$

At x=l,

$$u_2(l,t)=0 \qquad c_1' cos\lambda x + c_2' sin\lambda x = 0$$

$$\Rightarrow \qquad c_2' = -\frac{c_1' cos\lambda L}{sin\lambda L} \tag{26}$$

Solve these equation we got:

$$c_1 = a_l \tag{27}$$

$$c_2 = \frac{a_l(\frac{M\Omega^2}{\lambda EA} cos\lambda l_1 + sin\lambda l_1 - cos\lambda l_1 \frac{sin\lambda l_1 + \cot(\lambda l)\cos(\lambda l_1)}{cos\lambda l_1 - cot\lambda l sin\lambda l_1})}{sin\lambda l_1 \frac{sin\lambda l_1 + cot(\lambda l)cos(\lambda l_1)}{cos\lambda l_1 - cot\lambda l sin\lambda l_1} + cos\lambda l_1 - \frac{M\Omega^2}{\lambda EA} sin\lambda l_1} \tag{28}$$

$$c_1' = \frac{a_l cos\lambda l_1 + c_2 sin\lambda l_1}{cos\lambda l_1 - \cot(\lambda L)\sin(\lambda l_1)} \tag{29}$$

$$c_2' = -\frac{c_1' cos\lambda L}{sin\lambda L} \tag{30}$$

Bring in numerical value to equation, result shown in Figure 11.

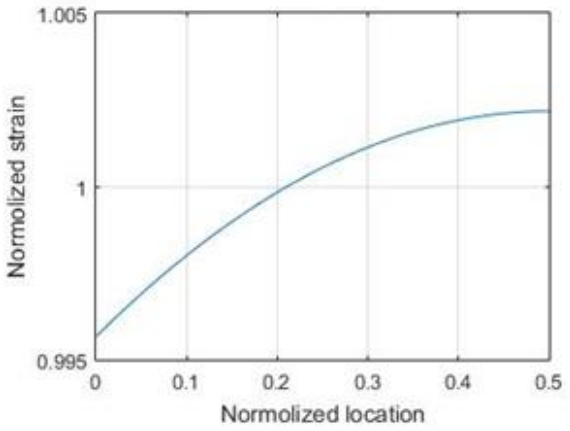

(a) Mode shape without lump mass

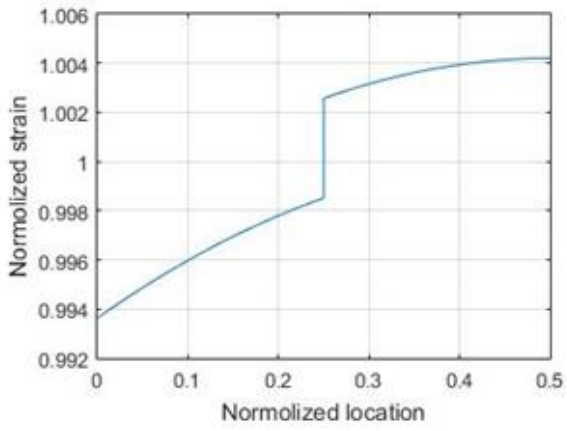

(b) Mode shape without 1 gram lump mass

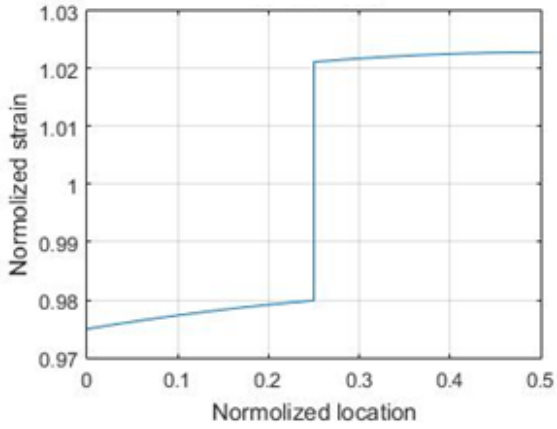

(c)Mode shape without 10 gram lump mass

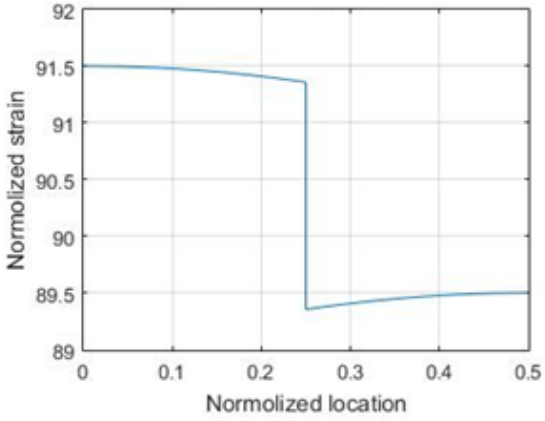

(d) Mode shape without 100 gram lump mass

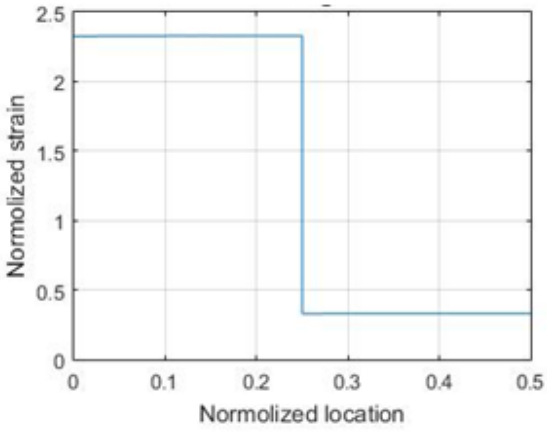

(e) Mode shape without 1 Kg lump mass

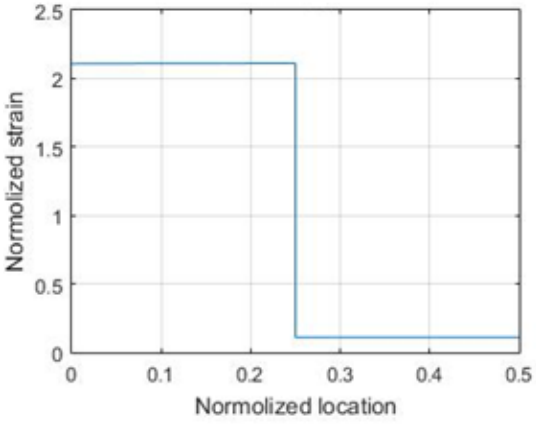

(f) Mode shape without 5 Kg lump mass

Figure 11 Lumped mass influence to battery tab longitudinal vibration

From figure 11we can find that while the mass less than 10 gram, the measured strain value almost no change.

This model based on the assumption that the influence of strain gauge wire can be evaluated by a rigid lumped mass on the battery tab. For real physics condition of the testing set up, there is no concentrated mass on the battery tab, the influence of battery tab wire mass may be better described as distributed mass around the area it attached on the battery tab. And the dimension of the area may not be neglect. The distributed mass probably has less influence to the battery tab compare with lumped mass, since the lumped mass model represents the worst working condition. Hence the conclusion is that the longitudinal vibration effect of strain gauge wire mass can be neglected.

The strain gauge wire mass influence to flexural vibration will be discussed in Chapter 5.

3.3 Study of Signal Conditioning System:

3.3.1 Study of Wheatstone Bridge Circuit

The strain gauge sensor converts the strain changes on the metal surface to the change of resistance of the gauge. The change of gauge resistance has a linear relationship with the change of strain. Shown in the following equation:

$$\Delta R = GF \times R_G \times \varepsilon \tag{31}$$

Where "GF" is the gauge factor, a parameter of the strain gauge which typically has a numerical value around 2. R_G is the resistance of the undeformed gauge, typically has 120 ohm or 350 ohm. ε is strain change.

For Wheatstone bridge circuit shown in Figure 12,

$$V_G = \left(\frac{R_2}{R_1 + R_2} - \frac{R_3}{R_3 + R_4}\right) V_s \tag{32}$$

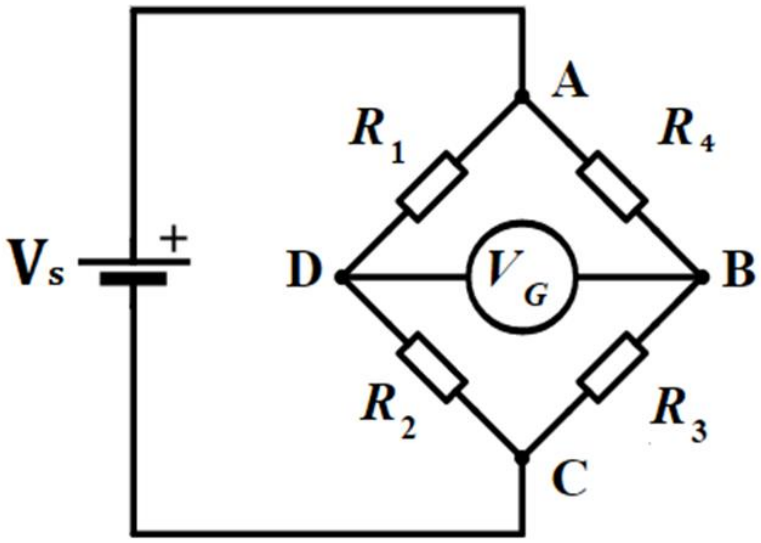

Figure 12 Wheatstone bridge circuit

Assume R_3 or R_4 replaced by strain gauge, combine equation (31) and equation (32), the relation curve between strain changes and output voltage and its linear curve fitting shown in the left 2 picture in Figure 13. We can find that the relation curve almost overlaps with its linear curve fitting. The right 2 picture in Figure 13 shows the difference between the relation curve and its linear curve fitting. The difference is less than 3 percent of measured strain. Hence we can assume the strain has a Proportional relation with the output voltage.

$$V_G = K \times \varepsilon \qquad (33)$$

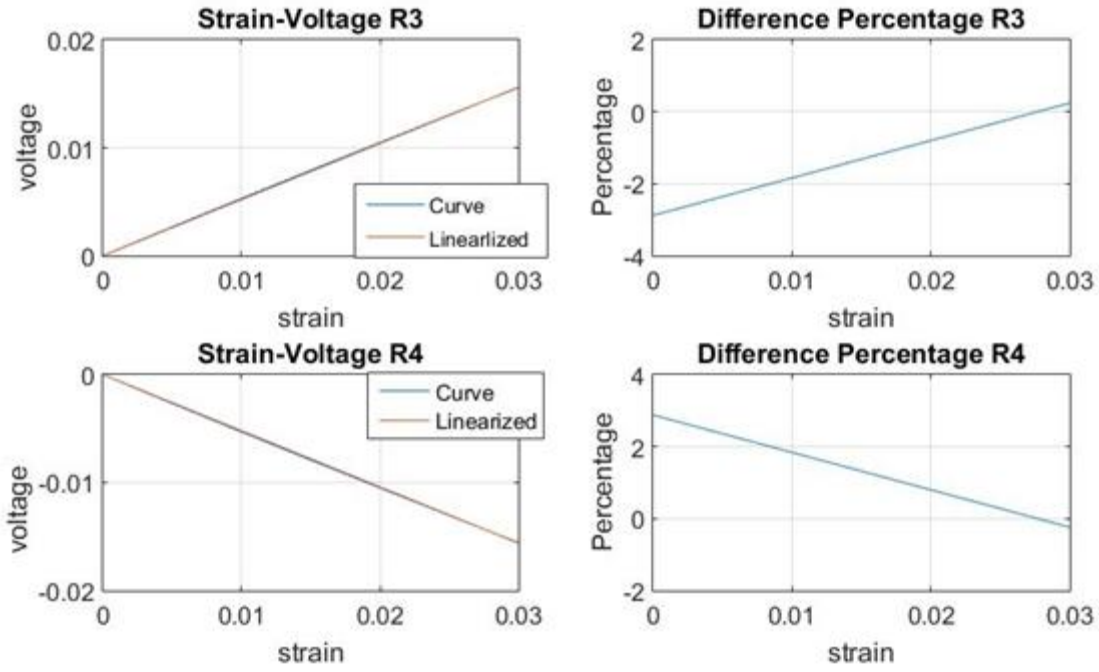

Figure 13 Relation between output voltage and strain change

The proportional relation between the strain and output voltage is very helpful. From equation (31) it can be found that for 1 micro-strain change, the resistance of strain gauge changes about 0.24 mΩ. Thus to use Equation (31) and Equation (32) to calculate the strain, very accurate resistance of the bridge circuit were needed. One problem is that the resistance of

commercial resistor always has tolerance and changes with temperature. Under the working condition, the current in the circuit probably different with the current under the circumstance in which measurement of resistance was conducted. Thus the heat generated under these two circumstances will be different. This cause temperature difference. Hence the measured resistance will different with the resistance at working condition. With the proportional relation, the accurate measurement of the initial resistance of the resistors in the bridge circuit is not needed.

With proportional relation between measured strain and output voltage, the fluctuation of R_1 ,R_2 and R_3 value compare with the standard value 120 Ω will changes the initial output voltage but we can still get a correct measured result. This may be hard to understand. For instance, in the Wheatstone bridge circuit shown in Figure 12. The static resistance of R_1, R_2 , R_3, R_4 were supposed to be 120 Ω. Due to manufacture variation, typically these resistance real value has 5% error. And after giving an excitation voltage, the current induced heat will cause temperature change which changes the initial resistance of these resistor. Thus the exact resistances of R_1, R_2 , R_3, R_4 are hard to know. With these not accurate resistances value bring into equation (31) and equation (32) will not get correct strain value. While giving the excitation voltage V_s to the bridge circuit, after several seconds the temperature around the circuit comes to steady state (not change anymore). Thus the resistance of the resistors in the bridge circuit will stay constant. Let's say at the temperature steady state $R_1 = 121\ \Omega$, $R_2 = 119\ \Omega$, $R_3 = 121\ \Omega$, R_4 be the strain gauge. With excitation voltage of 4 volts, Equation

$$V_G = \left(\frac{R_2}{R_1 + R_2} - \frac{R_3}{R_3 + R_4}\right) V_s \qquad (34)$$

Becomes

$$V_{G2} = \frac{119}{240} \times 4 - \frac{121}{121 + R_4} \times 4 \qquad (35)$$

Mark this as condition 2. And $R_1 = R_2 = R_3 = 120\ \Omega$ as condition 1.

$$V_{G1} = \frac{120}{240} \times 4 - \frac{120}{120+R_4} \times 4 \qquad (36)$$

Figure 14 shows the strain-output voltage relation of condition 1 (VG1) and condition 2(VG2).

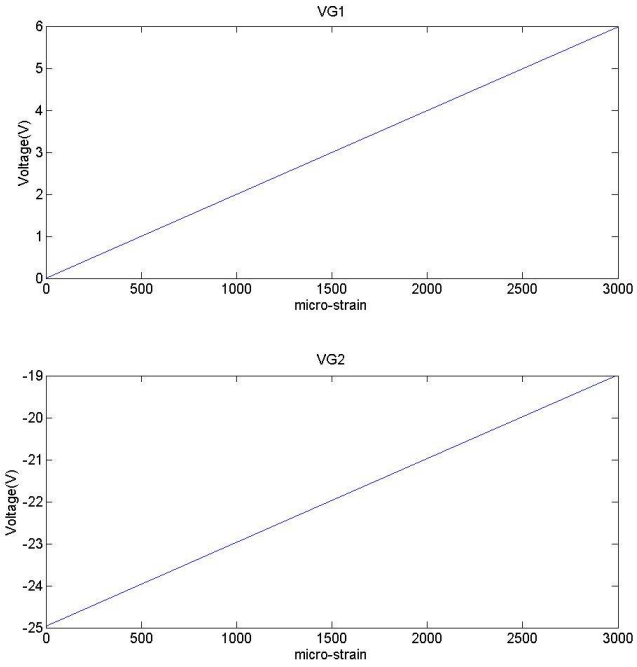

Figure 14 Strain-Voltage relations under different bridge circuit condition

From Figure 14 we can find that the relation strain-curve of condition 1 and condition 2 has the same slope. The strain-voltage relation can be expressed in following equations:

$$V_{G1} = K \times \varepsilon + C_1 \qquad (37)$$

$$V_{G2} = K \times \varepsilon + C_2 \qquad (38)$$

Where C_1, C_2 are constant.

In fact by change the resistance of the resistor in the bridge circuit, the output voltage at zero strain condition can always be zero. For example, change R_2 in condition 2 to 122 Ω.

$$V_{G3} = \frac{122}{243} \times 4 - \frac{121}{121 + R_4} \times 4 \qquad (39)$$

Figure 15 shows that with the tuning of R_2, at zero strain the output voltage is very close to zero. In the same way, tuning of R_1, R_3 have the same function. This is very important for amplifier circuit. Because the output range of the amplifier is about -10 Volts to 10 volts, if the initial output voltage at zero strain is 9 volt, the measurement strain range become less than 500 micro-strains. Hence in the circuit design, one resistor replaced by a potential meter. Before the testing, tuning the potential meter keeps the output voltage as close to zero as possible. And the strain-voltage relation does not change.

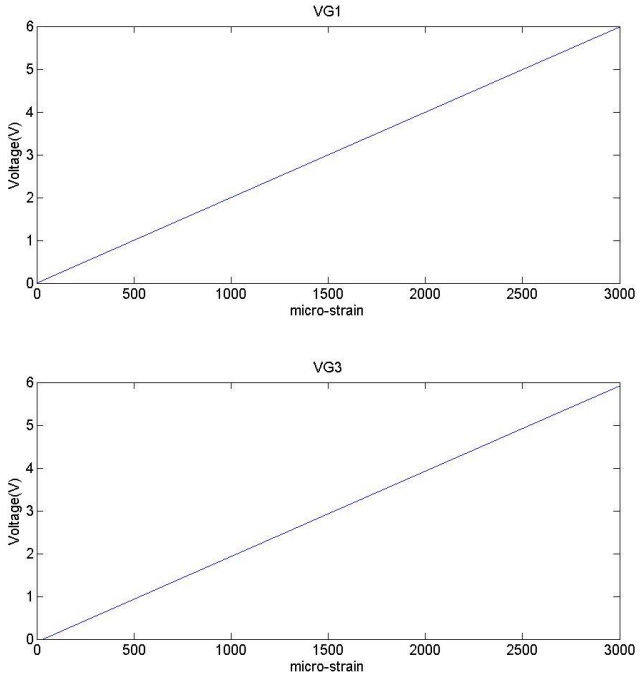

Figure 15 Tuned the initial output voltage by potential meter

Above discussion shows that the tolerance of the resistors and temperature effects do not influent the measurement result. To set up the bridge circuit, we can just use the cheap resistor.

Another issue about the bridge circuit is that it needs very accurate and stable excitation voltage. The NI-4110 DC power supply used in this study has a voltage sensitivity of 0.4 mV, which is accurate enough.

3.2.2 Amplifier Circuit

According to Figure 13, the output voltage of the bridge circuit will be several mV in the strain range of 0-3000 micro-strain. Hence amplification circuit is needed for signal conditioning. AD620 amplifier from Analogy Device Company was chosen to amplify the signal. The gain was set to be 1000 at 0 Hz. The circuit gain will decrease with the increase of signal frequency. Given a known signal with specific frequency by function generator as input to the amplifier, measure the output voltage of the amplifier. A frequency calibration curve was made.

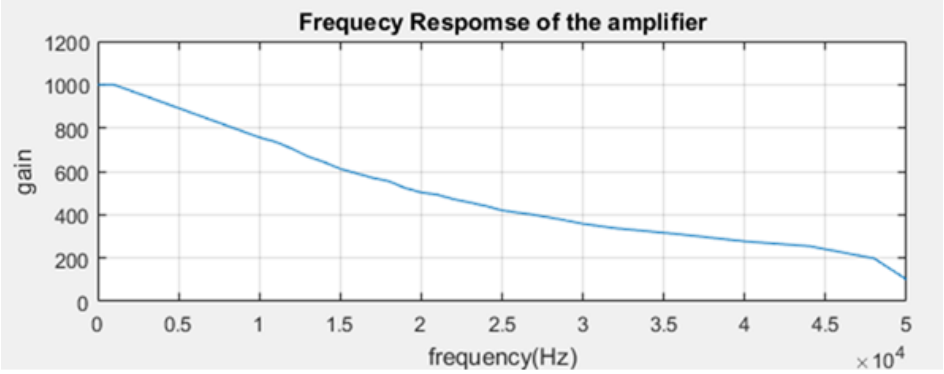

Figure 16 Amplifier gain frequency calibration curve

After experiment, first do an FFT to the data, multiply recover coefficient to the signal in different frequency bands according to the frequency calibration curve. Then do an inverse FFT get the real signal.

3.2.3 Anti-noise Design

In the industry environment, a lot of electric noise generated by motors, machines. To keep the signal-noise ratio of the measurement system reasonable, some actions need to be taken.

For static electric field noise, a closed conductor shell (Faraday cage) will provide very good shied to keep the circuit inside not influenced by the noise. The mechanism shown in Figure 17. A reverse electric static field will be generated on the shell cancel out the original static electric field.

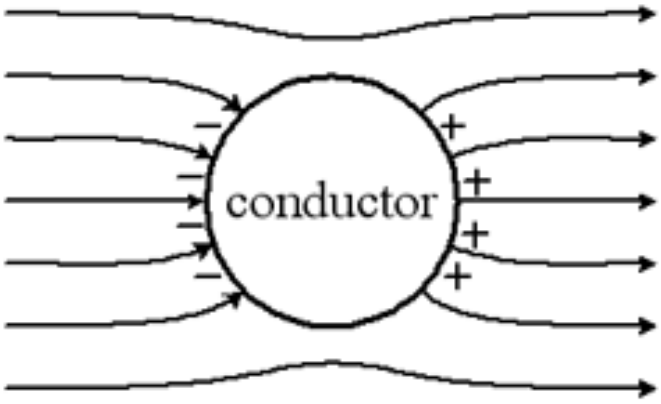

Figure 17 Electrostatic shielding

For electromagnetic shielding, barriers made of conductive or magnetic materials were used. Figure 18 shows the mechanism of the barriers. The transfer speeds of the electromagnetic wave are different in different materials. Thus while the wave transfer through the interface between different conductor, part of the wave will reflect back. Like the light transfer through the interface between air and water, while an incident electromagnetic wave come to the interface between air and conductor, part of the wave reflected back to the air. While the Refracted wave go through into the conductor, part of the wave energy will be absorbed by

material resistant. Then at the interface between the air and conductor inside of the box wave reflection happens again. After these reflection and absorption, the energy of electromagnetic wave which come into the space inside of the box decrease significantly.

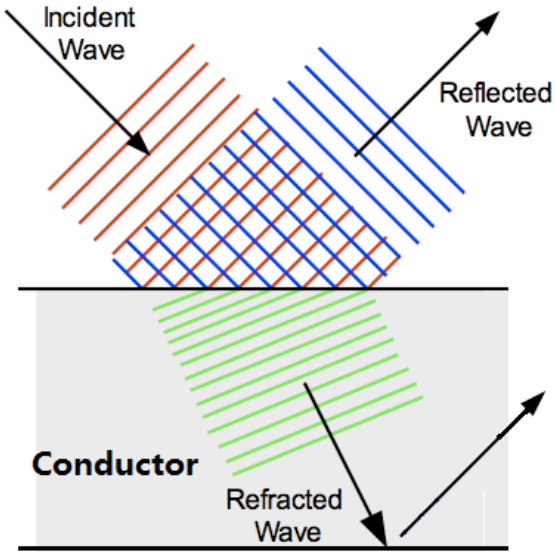

Figure 18 Mechanism of instrumentation box shield electromagnetic wave

Any holes in the instrumentation box must be significantly smaller than the wavelength of the radiation that is being kept out, or the enclosure will not effectively approximate an unbroken conducting surface. For this study, the high frequency noise generated by ultrasonic welding machine is 20 kHz. From equation (40) find that the wave length is 15 km. So do not need to worry the diffraction effect.

$$\lambda = \frac{v}{f} \qquad (40)$$

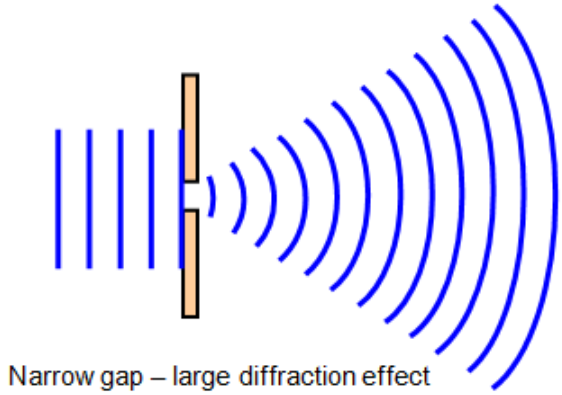

Figure 19 Electromagnetic diffraction effect of holes on instrumentation box

3.3 Data Acquisition and Synchronization of Measurement System

For the measurement experiments, several measurement equipments may involve include strain gauge, laser vibrometer, and high speed camera. Start and stop those machines one by one is not convenient, and bring difficulties for data correlation between different measurement methods. Hence the Synchronization of the measurement system is needed. A 24 Volts digital trigger signal generated by the PLC each time the foot paddle of welding machine was pushed. A relay transfers this 24 Volts signal to 5 volts and insulates the PLC from the measurement system.

For data acquisition system, NI-PXI-4472 data acquisition module was chosen to collect data from circuit to the computer. NI-PXI-4472 has sample rate up to 102.4 kHz, and 24-bit resolution ADCs voltage resolution.

A LabVIEW program was built for handling the Data Acquisition.

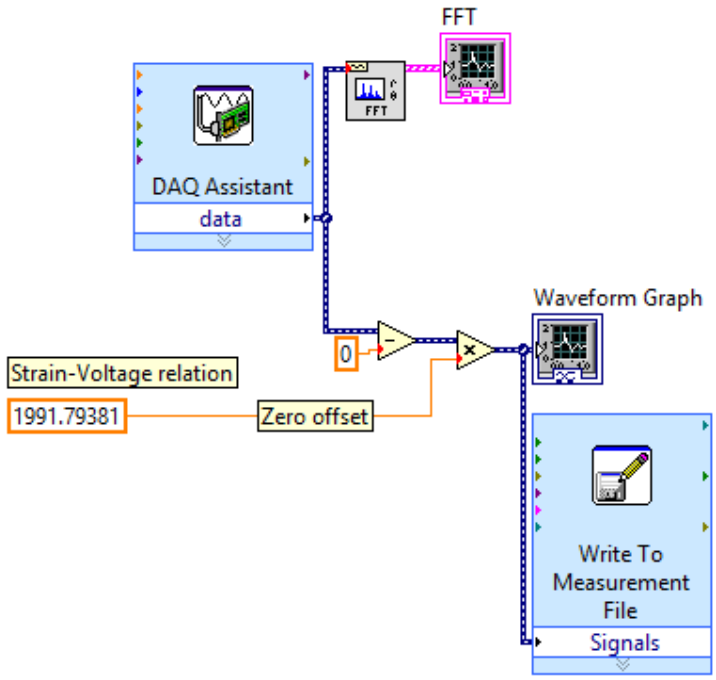

Figure 20 LabVIEW data acquisition program

3.4 Benchmark Experiments for Strain Gauge Measurement System

3.4.1 Static Test of Strain Gauge Measurement System

Attached strain gauge on an aluminum beam, as shown in Figure 21. Imply 1N force by 'IMADA' force gauge. The stress at the location where strain gauge attached to the beam can be calculated by equation

$$\sigma = \frac{My}{I_x} \quad (41)$$

Where $\sigma = E\varepsilon$, ε is strain.

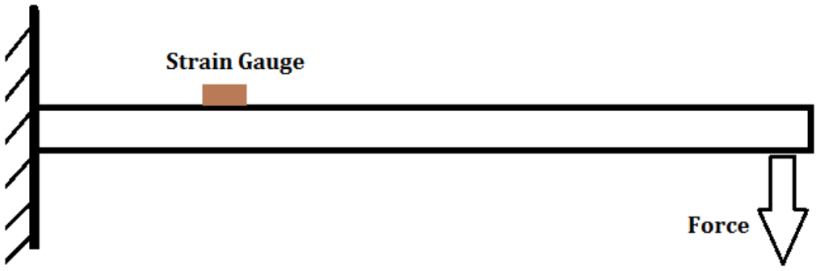

(a) Experiment set up

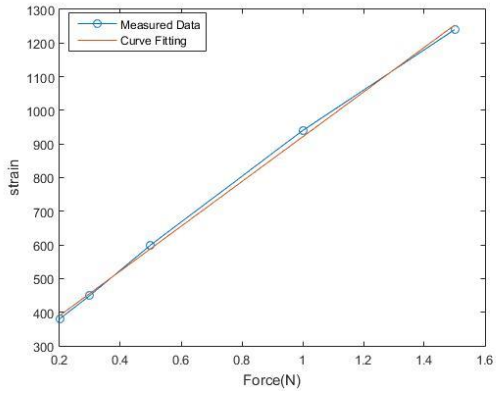

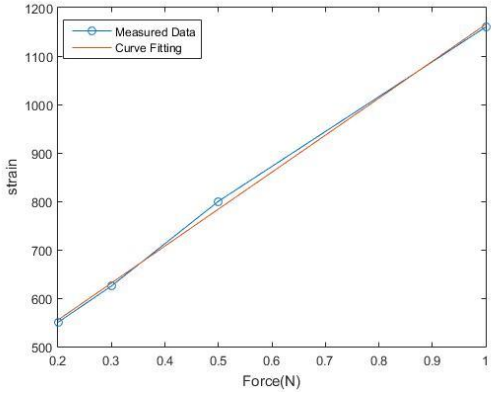

(b)Experiment 1 curve fitting result (c) Experiment 2 curve fitting result

Figure 21 Strain gauge benchmark experiment

The beam thickness: 1 mm, width: 23 mm, the distance between force to strain gauge 300 mm. From equation 10, we can calculate strain $\varepsilon = 652\ m\varepsilon$ with 1N force.

Apply curve fitting to experiment data, the Force/Strain linear relationship can be found. Use this relation, the experiment strain with 1N force can be calculated.

Test 1 Force	0.2 N	0.3 N	0.5N	1 N	1.5 N	Curve Fitting Result for 1 N Force
Micro-Strain	380	450	600	940	1240	**763**
Test 2 Force	0.2 N	0.3 N	0.5N	1 N		Curve Fitting Result for 1 N Force
Micro-Strain	550	625	800	1160		**664.4**
Analytical Solution						**652**

Table 1 Strain gauge static benchmark

The Experiments result very close to the analytical solution.

3.4.2 Compare Noise Level of Commercial Systems with Homemade System.

The homemade measurement system has better Signal-Noise ratio compare with one commercial system from Kyowa Company. Figure 22 shows the signal of strain gauge at static states (no strain change). The signal shown in Figure 22 can be regard as pure noise. The homemade system has about 80 micro-strain noise value. While the commercial measurement system from Kyowa Company has noise value about 160 micro-strain, about twice of the homemade system.

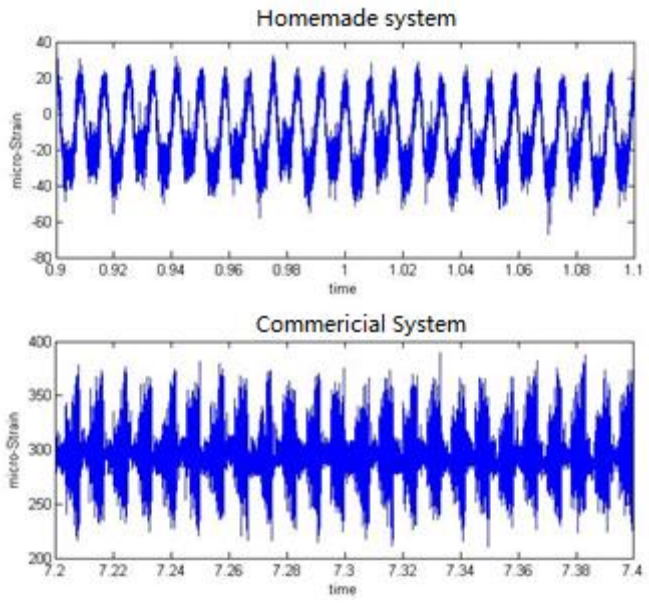

Figure 22 Compare noise level between homemade system and Kyowa commercial system

3.4.3 Correlate Laser Vibrometer Data with Strain Gauge Sensor:

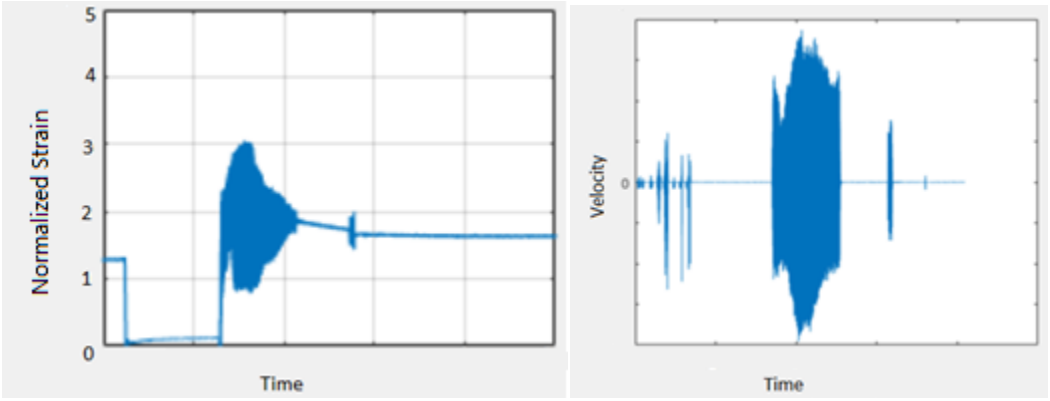

Figure 23 Correlate laser vibrometer data with strain gauge data

The laser vibrometer measured the flexural vibration of one point on the battery tab. While the strain gauge measured the strain induced by both flexural vibration and longitudinal

vibration. The response to the trigger signal of the strain gauge measurement system has a little bit delay compare with Laser vibrometer measurement system.

At the time period between 0 second and 1 second, the laser vibrometer shows some oscillation, while the strain gauge sensor did not capture the same information. At this period, the sonotrode start moves to clamp the battery tab. The impact force generated during when sonotrode collision with battery tab induced the oscillation of the whole system. Since this oscillation can be regard as rigid body motion of the whole system, the strain gauge did not capture anything. This suggestd that for studying the vibration of battery tab, the data from strain gauge is more reliable compared with laser vibrometer data.

Chapter 4 Experiment Test of Battery Tab Vibration Induced Strain

4.1 Longitudinal Vibration Induced Strain/Stress

To verify the analytical model and assumptions for battery tab vibration. Experiments were carried out. In this experiment, the assumption that the battery tab which is a metal plate can be modeled as a slender beam has been verified.

The experiment set up shown in Figure 24. A battery tab clamped straight between the welding tip and fixture.

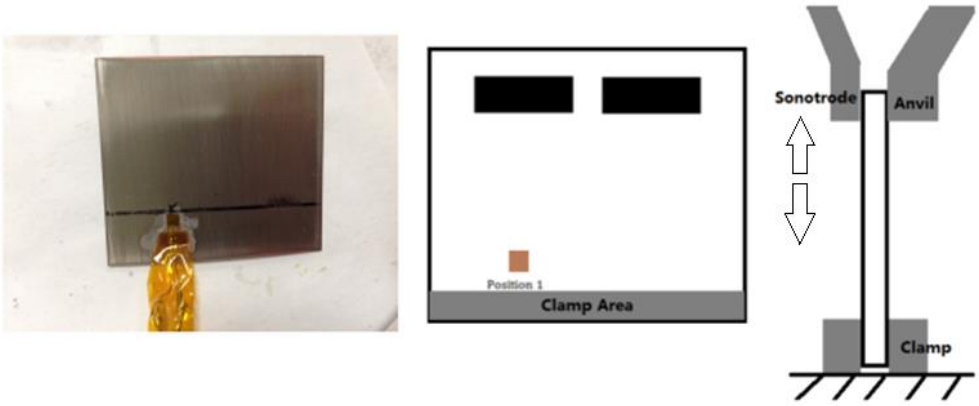

Figure 24 Ultrasonic welding measurement set up

The analytical solution can be calculated by equations in Chapter 2. The results shown in Figure 25. In the whole span the strain value not changes a lot.

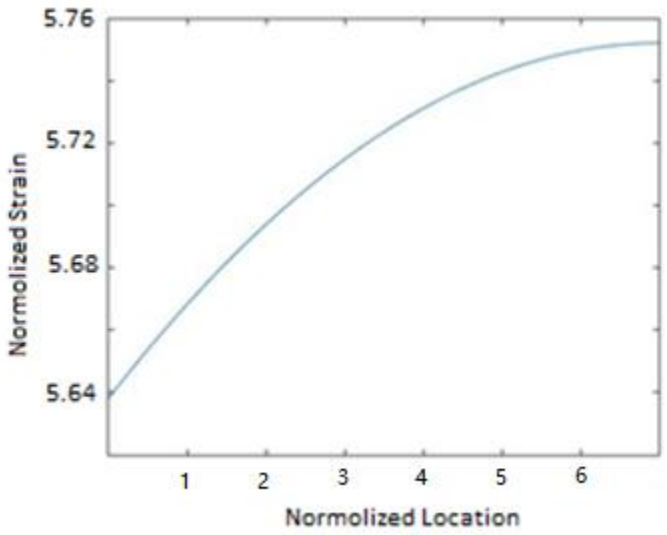

Figure 25 Calculated longitudinal vibration induced strain on battery tab

The experiment results shown in Figure 26,

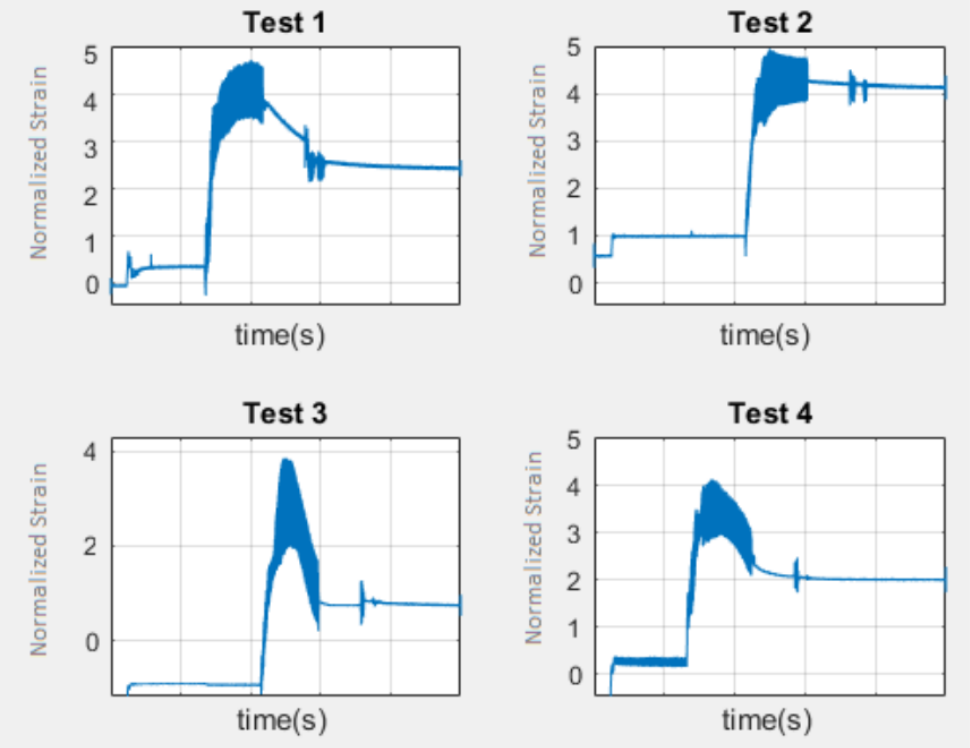

Figure 26 Measured strain value on battery tab

From Figure 26 we find the vibration induced strain peak-peak value shown in table 2

	Test 1	Test 2	Test 3	Test 4	Average	Analytical Solution
Peak to Peak micro-strain	1180	980	1150	1200	1127.5	1150

Table 2 Compare calculated strain with experiment data

The calculated dynamic strain value by the analytical model is very close to the experiment data. Hence the modeling assumptions were verified to be correct. Then we can use the model assumption build a more complex model to better predict the dynamic of battery tab.

4.2 Vibration Induced Strain/Stress Summary:

After the designed longitudinal vibration test, the vibration induced strain/stress has been measured under real battery pack assembly configuration. The results show that the vibration induced dynamic strain Peak-Peak value is in the safe range.

Chapter 5 Ways to Reduce Vibration of Battery Cell.

5.1 Tuned Mass Damper

Tuned mass damper[30, 31] has been used wildly in structures to reduce the vibration of the system include automotive, power transmission lines, buildings etc. In this study the tuned mass damper concept used to reduce the vibration on battery cell has been explored.

As shown in Figure 27, the battery tab modeled as a clamped beam, a lumped mass attached on the middle of battery tab. With proper location and mass value, the vibration of the battery can be reduced significantly. Analytical models were built to describe the dynamic and vibration of the battery tab with the lumped mass.

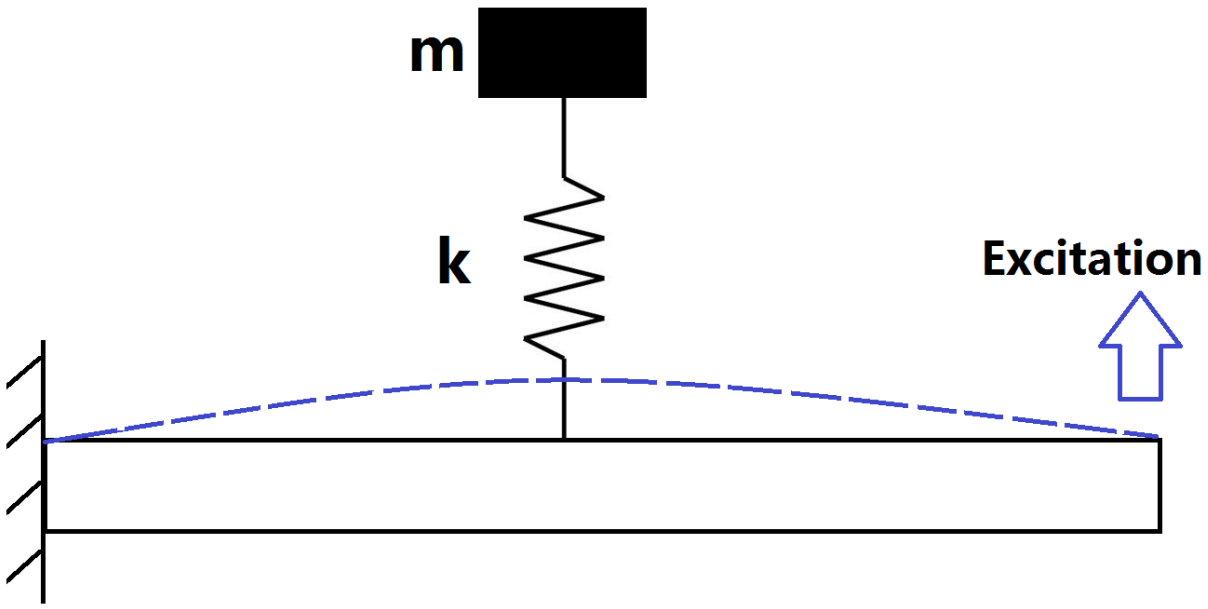

Figure 27 Tuned mass damper concept used to reduce battery tab vibration

5.1.1 Longitudinal Vibration:

In Chapter 3, the lumped mass influence to the battery tab vibration has been studied. It was found that while the lumped mass is big enough, the strain/stress value on the battery cell will reduce to very small value. Looks like while the vibration wave transfer to the location with lumped mass, most of the vibration energy be absorbed by the lumped mass.

5.1.2 Flexural Vibration:

Modeled the battery tab as a slender beam, as shown in figure 28**.** The lumped mass at location L1.

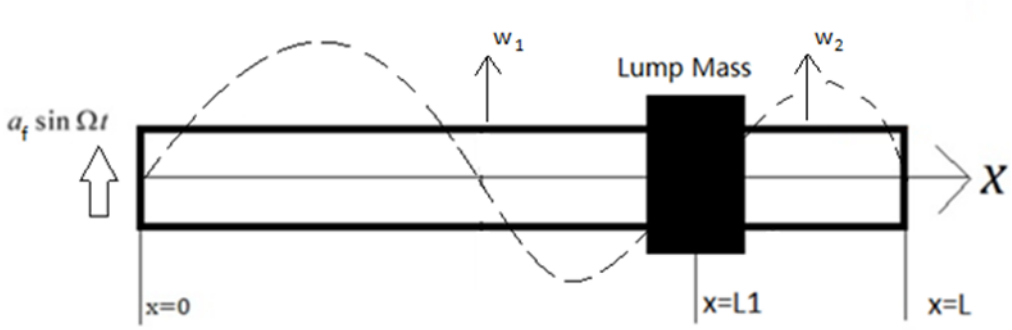

Figure 28 Lumped mass influence to flexural vibration

Assume the flexural displacement can be described by following equation:

$$w_1(x,t) = (C_1 cos\gamma x + C_2 cosh\gamma x + C_3 sin\gamma x + C_4 sinh\gamma x) sin\Omega t \quad (41)$$

$$w_2(x,t) = (C_1' cos\gamma x + C_2' cosh\gamma x + C_3' sin\gamma x + C_4' sinh\gamma x) sin\Omega t \quad (42)$$

Where $\gamma^2 = \sqrt{\frac{A}{I}}\frac{\Omega}{c_0}$

$$c_0 = \sqrt{\frac{E}{\rho}} = \sqrt{\frac{120\text{GPa}}{8950Kg/m^3}} = 3661.67$$

$$\Omega = 20KHz$$

$$I = \frac{dh^3}{12} = 3.27 \times 10^{-14} m^4$$

$$A = dh = 49mm * 0.2mm = 10^{-5}\ m^2$$

Hence

$$\gamma = 307.58$$

Boundary Condition:

At x=0, the slop of deflection is zero, and the deflection equal to the sonotrode motion

$$w_1(0,t) = a_f sin(\Omega t) \quad (43)$$

$$\frac{\partial w_1(0,t)}{\partial x} = 0 \quad (44)$$

At x=L1, neglect the rotation effect of the lump mass

$$w_1(l_1) = w_2(l_1) \quad (45)$$

$$w_1'(l_1) = w_2'(l_1) \quad (46)$$

$$M_2 - M_1 = \mathrm{I}_M \ddot{\theta} \quad (47)$$

$$M\frac{d^2w(l_1)}{dt^2} = Q_2(l_1) - Q_1(l_1) \tag{48}$$

Where

$$M_2 = -EI\frac{d^2w_2}{dx^2} \quad M_1 = -EI\frac{d^2w_1}{dx^2} \quad Q_2(l_1) = -EI\frac{d^3w_2}{dx^3}$$

At x=L,

$$w_2(L,t) = 0 \tag{49}$$

$$\frac{\partial w_2(L,t)}{\partial x} = 0 \tag{50}$$

From boundary condition we get 8 equations, Matlab is used to solve them numerically. This study select the Span 3 length as 62.5% of total length of the battery tab.

It was found that the influence of lump mass depends on the location it mounted.

Case 1: lumped mass fixed at the middle of the Span 3, no influence to tab vibration.

The figure 29 shows that while the lumped mass fixed at the middle of the Span 3, the lumped mass does not have any influence to the flexural vibration. This is because at the middle of Span 3, the flexural vibration has stationary modes, i.e. it will not vibrate at all at that point with or without the lumped mass.

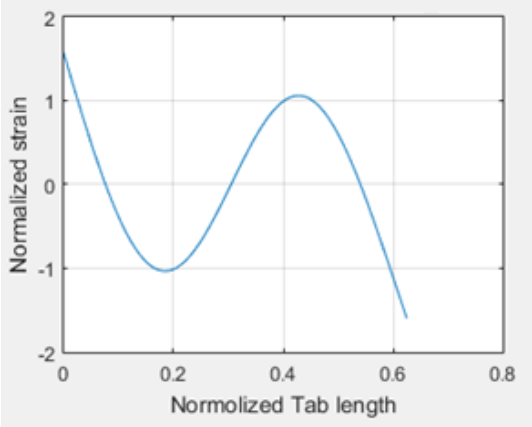

(a)

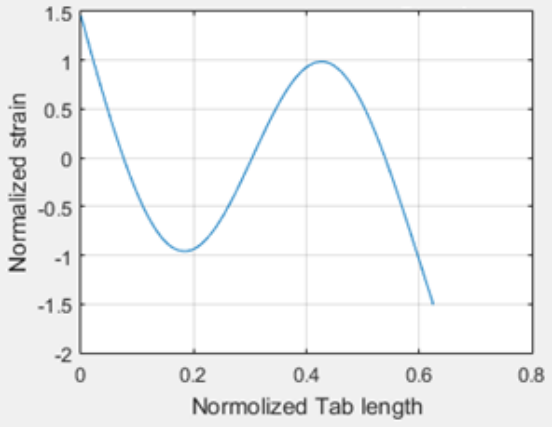

(b)

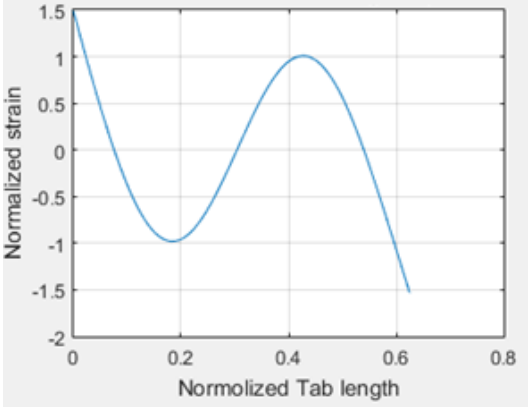

(c)

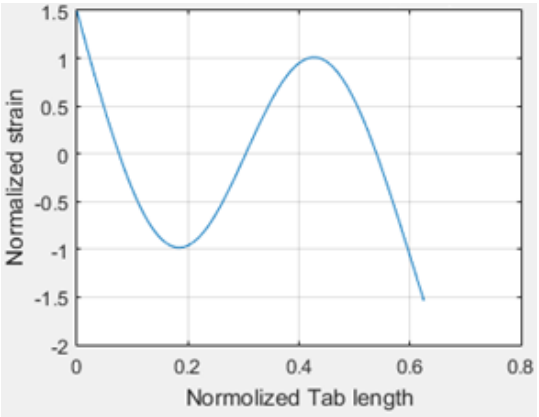

(d)

(a) Mode shape without lumped mass (b) Mode shape with 0.1 gram lumped mass

(c) Mode shape with 1 gram lumped mass (d) Mode shape with 10 gram lumped mass

Figure 29 Analysis of lumped mass fixed at the middle of the span 3

Case 2: lumped mass fixed at the normalized location 0.44 of the Span 3, reduces tab stress

The figure 30 shows that while the lumped mass fixed at location 0.44, it may have great influence to the flexural vibration of the battery tab. From the mode shape plot for battery tab strain without lumped mass we can find that at location 0.44 the vibration induced strain has relatively large amplitude. Thus while the lumped mass fixed at location 0.44 total length of the battery tab, form the equation of kinematic energy:

$$E = \frac{1}{2}mv^2 \tag{51}$$

The lumped mass will transfer the battery tab vibration elastic energy to kinematic energy. Thus reduce the amplitude of stress energy of the battery. Hence the strain value of the whole Span 3 reduces a lot.

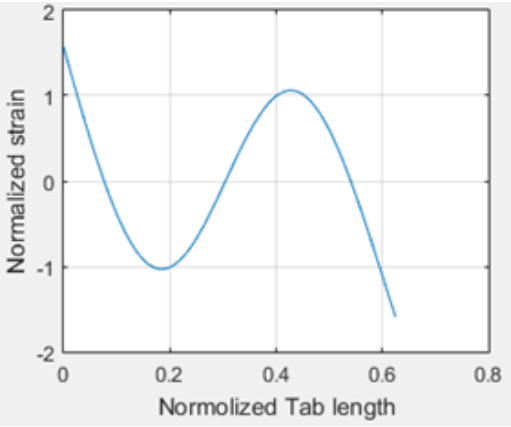

(a)

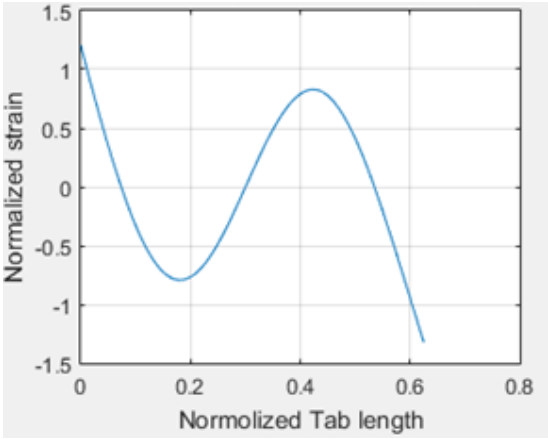

(b)

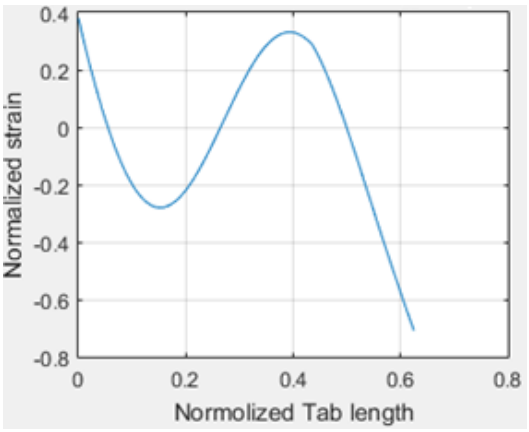

(c)

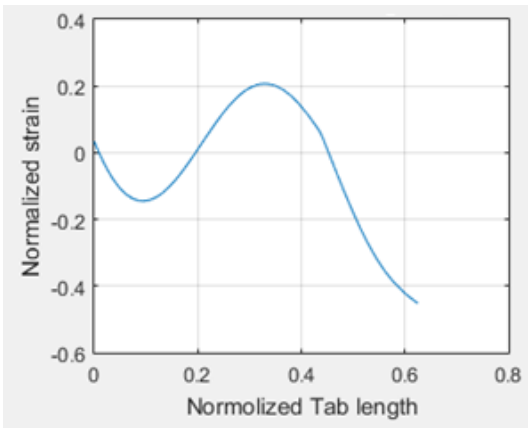

(d)

(a) Mode shape without lumped mass

(b) Mode shape with 0.1 gram lumped mass

(c) Mode shape with 1 gram lumped mass

(d) Mode shape with 10 gram lumped mass

Figure 30 Analysis of lumped mass fixed at span 3 location 0.44

Case 3: lumped mass fixed near the end of battery tab, no influence to tab vibration.

If the lumped mass fixed near the end of battery tab, it does not influence the dynamic and vibration of battery. As shown in Figure 31. It is easy to understand this phenomenon. Near the fixed boundary, the vibration amplitude is small, thus the vibration amplitude of the lumped mass is small, thus the lumped mass just absorb a small amount of vibration energy.

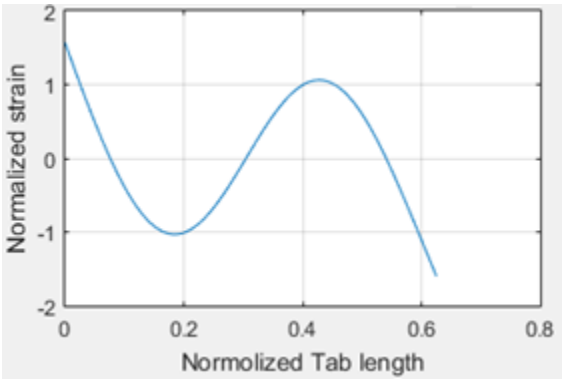

(a)

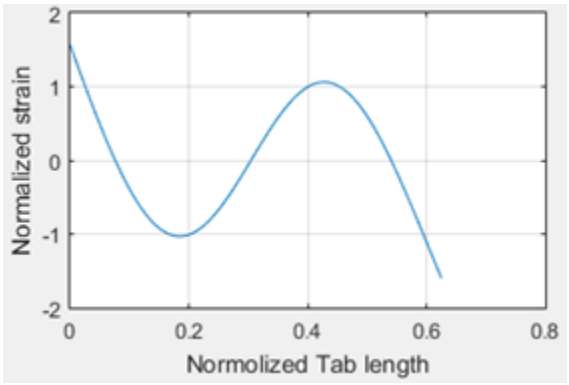

(b)

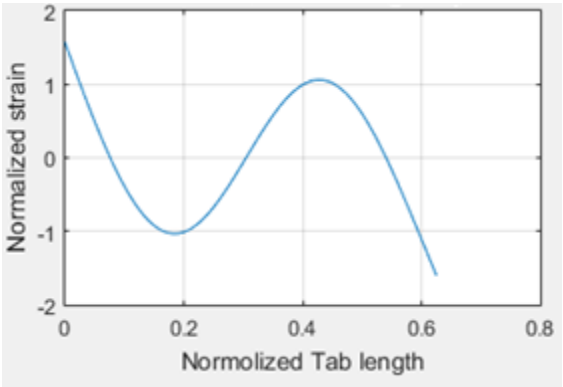

(c)

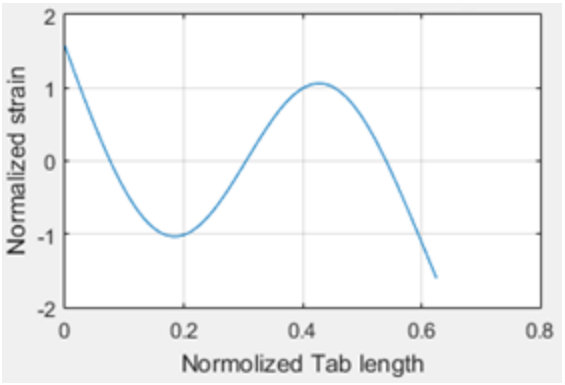

(d)

(a) Mode shape without lumped mass (b) Mode shape with 0.1 gram lumped mass

(c) Mode shape with 1 gram lumped mass (d) Mode shape with 10 gram lumped mass

Figure 31 Analysis of lumped mass fixed near the right end of battery tab

From the numerical result we can get 3 conclusions:

1. The flexural vibration amplitude is more sensitive to lumped mass compared with longitudinal vibration.
2. The influence of lumped mass to flexural vibration depends on its locations on the battery tab.
3. The lumped mass effect may influence the strain gauge measurement for flexural vibration, in experiment, the mount and wire connection of strain gauge should be manipulate carefully.

5.2 Add Clamp in the Middle of Battery Tab Span

The study shown in Chapter 2 shows that if the tab end modeled as free boundary condition, the strain value near the tab boundary will reduce to almost zero, i.e. the rigid body motion dominates the dynamic of battery tab during the ultrasonic welding.

If the battery cell is clamped to ground between the tab end and 'S' bend, the vibration of the battery tab part which is at the right of the 'S' bend can be modeled as free end boundary vibration. Because compare to tab clamp to ground, the battery connect with a battery pack frame not tight. Through this method the high strain/stress may concentrate at the clamped position, the battery cell will be protected.

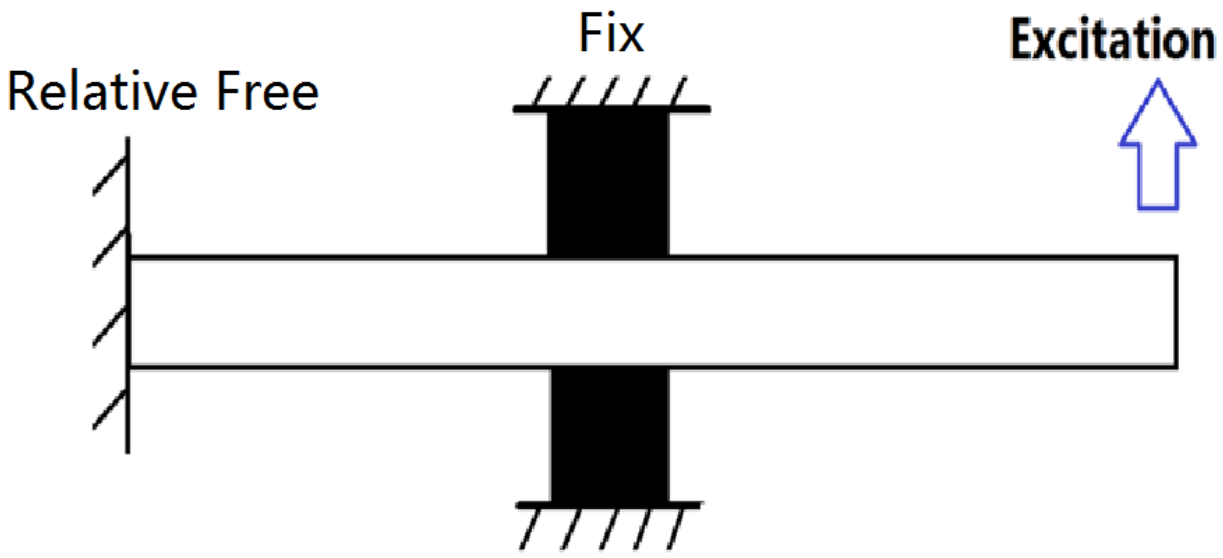

Figure 33 Add clamp at the middle of battery tab

Chapter 6 Conclusion and Future Works

From the above discussion, we can draw the following conclusions:

1. The modeling assumption that the battery tab is modeled as a thin beam is suitable, similar to [3].
2. Strain gauge sensor is useful for battery tab strain measurement.
3. The vibration induced dynamic stress value is in the safe range of metal strength.
4. Add clamp in the middle of battery tab and apply tuned-mass damper concept may reduce the strain value at the battery cell.

Future work:

1. An experimental study correlating battery tab stress with manufacture configuration parameters includes tab bending angle, tab length.
2. Experimental study of tuned mass damper concept used to decrease vibration in the battery cell.
3. Build a more complicated model to describe the battery tab dynamic better.

References

1. Lee, S.S., et al. *Joining technologies for automotive lithium-ion battery manufacturing - A review*. in *ASME 2010 International Manufacturing Science and Engineering Conference, MSEC 2010, October 12, 2010 - October 15, 2010*. 2010. Erie, PA, United states: American Society of Mechanical Engineers.
2. Lee, S.S., et al., *Characterization of joint quality in ultrasonic welding of battery tabs.* Journal of Manufacturing Science and Engineering, Transactions of the ASME, 2013. **135**(2).
3. Kang, B., W. Cai, and C.-A. Tan, *Dynamic Stress Analysis of Battery Tabs Under Ultrasonic Welding.* Journal of Manufacturing Science and Engineering, 2014. **136**(4): p. 041011-041011.
4. Doumanidis, C. and Y. Gao, *Mechanical modeling of ultrasonic welding.* WELDING JOURNAL-NEW YORK-, 2004. **83**(4): p. 140-S.
5. Zhang, C.S. and L. Li, *A coupled thermal-mechanical analysis of ultrasonic bonding mechanism.* Metallurgical and Materials Transactions B, 2009. **40**(2): p. 196-207.
6. De Vries, E., *Mechanics and mechanisms of ultrasonic metal welding*. 2004, The Ohio State University.
7. Rozenberg, L. and A. Mitskevich, *Ultrasonic Welding of Metals.* Physical Principles of Ultrasonic Technology, 1973. **1**(Part 2).
8. Devine, J., *Joining metals with ultrasonic welding.* MACH DES, 1984. **56**(21): p. 91-95.
9. Flood, G., *Ultrasonic energy welds copper to aluminium.* Welding Journal, 1997. **76**(1).
10. Lee, D., E. Kannatey-Asibu, and W. Cai, *Ultrasonic welding simulations for multiple layers of lithium-ion battery tabs.* Journal of Manufacturing Science and Engineering, 2013. **135**(6): p. 061011.
11. Viswanath, A.G., et al., *Numerical study of gold wire bonding process on Cu/low-k structures.* IEEE Transactions on Advanced Packaging, 2007. **30**(3): p. 448-456.
12. Siddiq, A. and E. Ghassemieh, *Theoretical and FE analysis of ultrasonic welding of aluminum alloy 3003.* Journal of manufacturing science and engineering, 2009. **131**(4): p. 041007.
13. Lee, S.S., et al., *Parasitic vibration attenuation in ultrasonic welding of battery tabs.* The International Journal of Advanced Manufacturing Technology, 2014. **71**(1-4): p. 181-195.
14. Jagota, A. and P. Dawson, *The influence of lateral wall vibrations on the ultrasonic welding of thin-walled parts.* Journal of Engineering for Industry, 1987. **109**(2): p. 140-147.
15. Bongsu, K., W. Cai, and T. Chin-An, *Vibrational energy loss analysis in battery tab ultrasonic welding.* Journal of Manufacturing Processes, 2014. **16**(2): p. 218-32.
16. Kang, B., W. Cai, and C.-A. Tan. *Dynamics of Battery Tabs Under Ultrasonic Welding*. in *ASME 2013 International Design Engineering Technical Conferences and Computers and Information in Engineering Conference*. 2013. American Society of Mechanical Engineers.

17. Bell, J.R. and S. Rothberg, *Laser vibrometers and contacting transducers, target rotation and six degree-of-freedom vibration: what do we really measure?* Journal of Sound and Vibration, 2000. **237**(2): p. 245-261.
18. Pedrini, G., W. Osten, and M.E. Gusev, *High-speed digital holographic interferometry for vibration measurement.* Applied optics, 2006. **45**(15): p. 3456-3462.
19. Serridge, M. and T.R. Licht, *Piezoelectric accelerometer and vibration preamplifier handbook*. 1986: Bruel & Kjaer.
20. Albarbar, A., et al., *Performance evaluation of MEMS accelerometers.* Measurement, 2009. **42**(5): p. 790-795.
21. Baik, S., et al., *Theoretical analysis of flexible strain-gauge sensor with nanofibrillar mechanical interlocking.* Current Applied Physics, 2015. **15**(3): p. 274-8.
22. Hilal Muftah, M., et al., *An improved strain gauge-based dynamic torque measurement method.* International Journal of Circuits, Systems and Signal Processing, 2013. **7**(1): p. 66-73.
23. Qingfeng, X. and F. Quail, *Principles and validation of strain gauge shunt design for large dynamic strain measurement.* Sensors and Actuators A: Physical, 2016. **241**: p. 124-34.
24. Stepanova, L.N., et al., *Microprocessor multichannel strain-gauge systems for dynamic tests of structures.* Sensors and Systems, 2011(8): p. 29-34.
25. Graff, K. *Process applications of power ultrasonics-a review*. in *1974 Ultrasonics Symposium*. 1974. IEEE.
26. Ueda, K. and A. Umeda, *Dynamic response of strain gages up to 300 kHz.* Experimental Mechanics, 1998. **38**(2): p. 93-98.
27. Hoffmann, K., *Applying the wheatstone bridge circuit*. 1974: HBM.
28. Cowles, V.E., et al., *A quarter wheatstone bridge strain gage force transducer for recording gut motility.* The American journal of digestive diseases, 1978. **23**(10): p. 936-939.
29. Dally, J.W., W.F. Riley, and K.G. McConnell, *Instrumentation for engineering measurements.* Engineering Analysis, 1984. **1**(2): p. 119.
30. Lai, M.-L., *Tuned mass damper*. 1999, Google Patents.
31. Soto, M.G. and H. Adeli, *Tuned mass dampers.* Archives of Computational Methods in Engineering, 2013. **20**(4): p. 419-431.

ABSTRACT

EXPERIMENTAL STRAIN MEASUREMENT IN ULTRASONIC WELDING OF BATTERY TABS

by

CHEN CHEN

Advisor: Dr. Chin An Tan

Major: Mechanical Engineering

Degree: Master of Science

AUGUST 2016

Lithium-ion battery is one the most popular types of batteries currently used in electric vehicles. To meet the power requirement, hundreds of Lithium ion battery cells are connected together before being assembled into a battery pack. Ultrasonic welding is the most widely used joining technology to connect battery cells together. In an ultrasonic welding process, high frequency oscillation is used to generate small relative motions between sheet metals to be welded, and produce solid-state bonds between the sheet metals clamped under pressure. One of the major issues for battery pack ultrasonic welding is that sometimes the welding process damages the battery cell. It is hypothesized that, during the ultrasonic welding process, high frequency vibrations of battery tabs may transfer vibration energy into the battery cell, inducing high stresses and even causes damages at the interior joints of the battery cell. In this study, an analytical model to describe the vibration of battery tabs was developed. Experimental data shows good correlation to the analytical model in the stress value. For the experimental measurement, a signal conditioning and data acquisition system was developed which was

shown to have good signal-noise ratios when compared to a commercially available measurement system.

AUTOBIOGRAPHICAL STATEMENT

Chen Chen is interested in vehicle dynamics which involves simulation and control of multi-link dynamic system. His specific areas of interest include dynamics, vibration, control and soft robotic.

Education:

Wayne State University	Detroit, MI	2016
Master of Science in Mechanical Engineering		
South China University of Technology	Guangzhou, China	2015
Bachelor of Science in Mechatronic Engineering		